Evolution of microstructures during the solidification of 304 austenitic stainless steel

K. Mukunthan, F. DeSylva, L. Strezov, J. Herbertson

There is limited scope for microstructure refinement after solidification in the emerging strip casting processes, which makes the understanding of the evolution of microstructures during solidification important in commercialising these technologies. The present study examined solidification under controlled laboratory conditions designed to simulate the meniscus region and the liquid pool of a twin roll caster. A strong link between initial heat transfer, surface nucleation and subsequent microstructures was established, suggesting that the control of initial melt/substrate contacting conditions and heat transfer is imperative in controlling the final microstructures. This has been demonstrated experimentally during the solidification of 304 austenitic stainless steel through the effects of different substrate surface textures and the influence of surface active sulphur on the evolving microstructures.

The austenite grains had elongated columnar shapes made up of families of dendrites growing opposite to the local direction of heat flow. Austenite grain widths were found to closely reflect the surface nucleation spacings, typically in a 1:1 correlation, with some cases of grain multiplication associated with non-uniform thermal fields around contact points.

Parole chiave: acciaio inox, solidificazione, metallografia

INTRODUCTION

The process of microstructure evolution in strip casting is fundamentally different from that in conventional hot strip mills. Slab products undergo a large degree of reduction, which breaks up the coarse cast structure through repetitive recrystallisation processes, resulting in significant refinement of final hot band microstructures. In contrast, the scope for microstructure refinement after solidification is severely limited for the strip cast route with cast section thicknesses of 2 mm and less, and consequently, effective control of as-cast microstructures is critically important for strip cast product development (1,2). The second aspect that distinguishes the strip cast route from that of the slab cast route is the significance of the surface contacting conditions on the overall microstructure development. For conventionally produced thick or thin slabs, the surface solidification layers correspond to only a small fraction of the total thickness. In contrast, for directly cast thin strips, the surface contacting conditions can influence the entire through thickness microstructure (2). For strip cast, low carbon steel there is the possibility of obtaining some microstructure refinement through solid state phase transformations. For example, considerable microstructure refinement can be achieved through low temperature austenite decomposition (2,3,4). However, very little scope exists for microstructure refinement by solid state transformations for strip cast austenitic and ferritic stainless steels (5,6), making control of as cast microstructures even more important for successful product development.

The importance of the first few milliseconds of melt/substrate contact and its effects on the rates of interfacial heat transfer during solidification is now recognised. Strezov and Herbertson (7) have shown that heat flux changes were associated with changes in nucleation density at the strip surface, and reflected in the surface and cross-sectional solidification dendritic structures. A more detailed understanding of the link between the surface nucleation density and the evolving microstructure, as defined by the cross-sectional austenite grain size, was the driver of the current work. Microstructure development during solidification was investigated under controlled laboratory conditions designed to simulate the conditions encountered in the meniscus region and the pool of a twin roll caster. The aim was to study the interdependence between the transient heat fluxes, surface nucleation densities and the final solidification grain structures with particular focus on linking the cross sectional grain structure to the surface nucleation pattern. This has been accomplished experimentally, by the use of specially designed substrate textures to control melt/substrate contact and by the additions of surface active agents such as sulphur in the melt. The strong influence the substrate texture had on the cross-sectional grain development could be interpreted in terms of the nucleation pattern at the surface and the relative uniformity of the temperature fields around the melt/substrate contact points.

K. Mukunthan, F. DeSylva, L. Strezov and J. Herbertson*
BHP Minerals Technology, PO Box 188, Wallsend, NSW 2287, Australia
** Now, Director, Skye Point Innovation, Australia*

Paper presented at the 7th European Conference EUROMAT 2001, Rimini, 10-14 June 2001, organised by AIM

EXPERIMENTAL DETAILS

Immersion Apparatus

An immersion apparatus capable of simulating initial contacting conditions pertinent to twin roll casting was used to produce metal samples under controlled solidification conditions for metallographic analysis. The experimental apparatus, details of which have previously been reported (7), was capable of millisecond resolution of interfacial heat transfer. The experiments were performed with various substrates embedded in a moving paddle, which was immersed in the furnace containing 304 austenitic stainless steel melt

C	Mn	Si	S	Cr	Ni	Cu	N
0.05	1.17	0.32	0.006 – 0.07	17.05	9.15	0.40	0.06

Table 1 - Typical melt composition of 304 austenitic stainless steel (wt %)
Tabella 1 - tipica composizione dell'acciaio inossidabile austenitico 304 fuso

with a prescribed velocity and residence time. The samples were cooled by a blast of N_2 gas immediately after the paddle had been withdrawn from the melt.

Experimental Conditions

The stainless steel melt chemistry shown in Table 1 corresponds to a low Cr/Ni equivalent ratio of approximately 1.48 (8,9). All of the microstructures presented in this paper correspond to this melt chemistry. Some samples produced with higher Cr/Ni ratios (up to a maximum of 1.92) were also used in the overall analysis to extend the range of correlations. Stainless steel melt chemistry with Cr/Ni ratios of less than 1.5 was identified as particularly suitable for this study as it solidifies predominantly to the austenite phase, commencing at around 1450∞C, and remains austenitic on cooling to ambient temperature (8,9). Furthermore, revealing the surface nucleation sites, dendritic structures and austenite grain boundaries in these samples is relatively easy due to their high level of microsegregation.
Clarifying the fundamental relationship between surface nucleation and microstructures was considered to be much less complex with 304 stainless than with low carbon steels, where the final microstructure is influenced by several solid state phase transformations (delta - austenite - ferrite). In addition, obtaining sufficient contrast to reveal dendritic as well as original solidification grain structures that allows for good quantitative characterisation is difficult for low carbon steels.
Primary experimental variables in this study were melt chemistry and substrate surface texture. The effect of sulphur, a surface active element, was investigated. The chrome coated copper substrates used in these experiments had either a smooth surface finish of 0.1 µm Ra or a textured surface finish corresponding to 180 µm pitch and 25 µm depth produced by machining ridges parallel to the dipping direction. Special experiments were carried out with flat top pyramid textures to control contact areas and spacings. The furnace atmosphere was either high purity argon or nitrogen, the melt superheat was around 125∞C (melt temperature of 1575∞C), the paddle immersion velocity was 1 m/s with a residence time of 190 ms in the melt and the initial substrate temperature was around 110∞C.

Heat Transfer Measurements and Microstructure Characterisation

Thermal phenomena occurring during solidification was measured using two 0.25 mm diameter, type K thermocouples placed within each substrate at a depth of 500 to 600 µm below the substrate surface. The temperature data acquired was used to calculate transient heat fluxes by employing an inverse heat conduction algorithm. Information on thermocouple positioning, data acquisition rates, inverse heat transfer calculations and data reproducibility has been presented previously (7).
The nucleation pattern and solidification structures on the surfaces of the solidified samples were studied without etching. Dendritic and grain structures in the cross-sections of the solidified samples were revealed by electrolytic etching in 60% nitric acid solution. A lighter etching together with a higher magnification (at least 500 times) was found to be beneficial in revealing the austenite grain boundaries. The contrast of the dendritic structure could be enhanced with an interference contrast attachment using oblique illumination.

RESULTS AND DISCUSSION

Surface Nucleation Behaviour and Transient Heat Fluxes

Surface solidification structures observed for the samples solidified with the smooth and the textured substrates demonstrated very different nucleation patterns. Nucleation appeared to have occurred in a random manner on the smooth substrate and, in general, these samples exhibited coarse surface dendrites, together with correspondingly coarse nucleation spacing. With increasing sulphur, a progressive reduction in nuclei spacing was observed. Surface solidification structures shown in Fig. 1 (a) and (b), obtained for samples solidified on the smooth substrate with sulphur

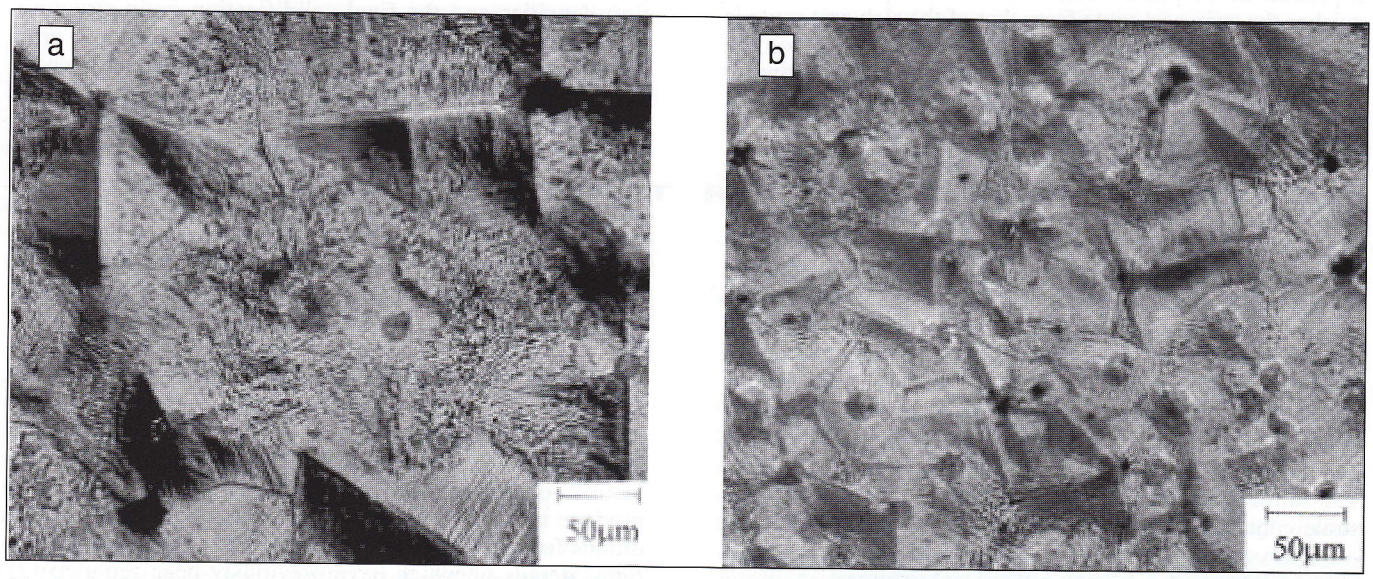

Fig. 1 - Surface solidification structures of the samples solidified on the smooth substrate (a) 0.015 wt% S and (b) 0.03 wt% S (Note that the nucleation points have been highlighted for clear identification)

Fig. 1 - Strutture della solidificazione superficiale dei campioni solidificati su substrato liscio (a) 0,015 peso % S e (b) 0,03 peso % S (I punti di nucleazione sono stati evidenziati per una più chiara identificazione)

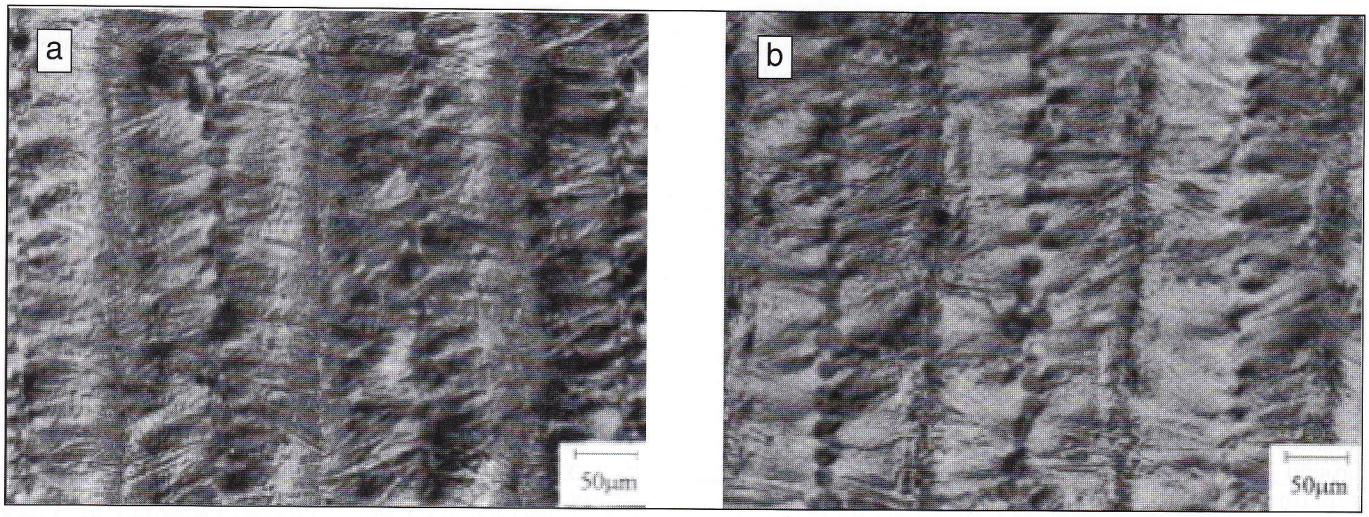

Fig. 2 - Surface solidification structures of the samples solidified on the ridge textured substrate (a) 0.006 wt% S and (b) 0.03 wt% S (Note that the nucleation points along selected ridges have been highlighted for clear identification)

Fig. 2 - Strutture della solidificazione superficiale dei campioni solidificati su substrato rugoso (a) 0.006 peso % S e (b) 0.03 peso % S (I punti di nucleazione sono stati evidenziati per una più chiara identificazione)

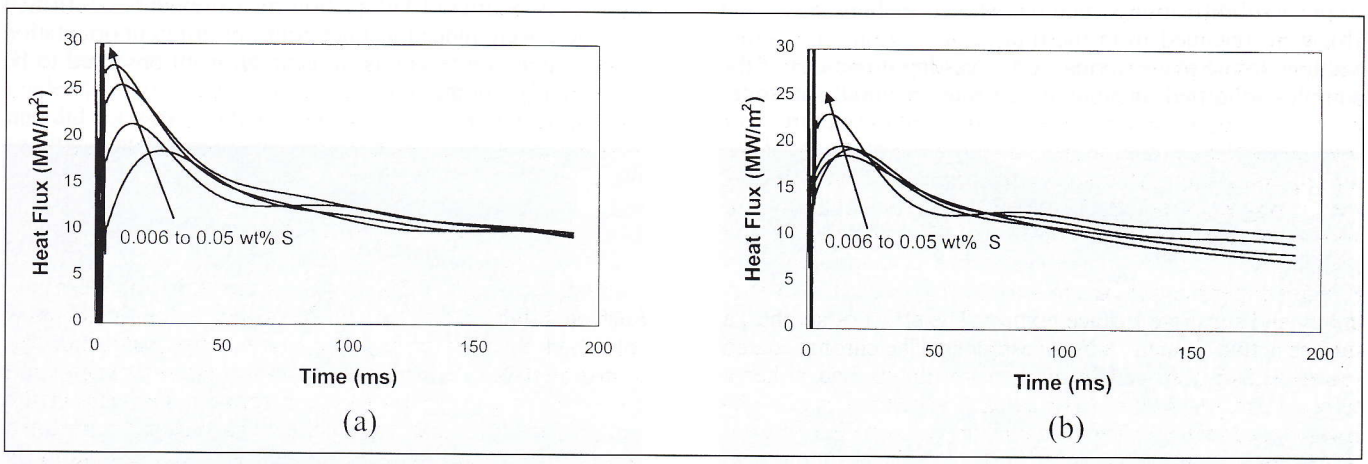

Fig. 3 - Transient heat flux curves obtained for the samples solidified on (a) smooth and (b) ridge textured substrates with melts containing 0.006, 0.015, 0.03 and 0.05 wt% S

Fig. - Curve del flusso di calore transitorio ottenute per i campioni solidificati su substrato liscio (a) e rugoso (b) con fusioni contenenti 0,006, 0,015, 0,03 e 0,05 peso % S

contents of 0.015 and 0.03 wt%, clearly illustrate this. The corresponding surface structures obtained for the 180x25 µm ridge textured substrate, with sulphur contents of 0.006 and 0.03 wt%, are shown in Fig. 2 (a) and (b). These microstructures exhibit a definite pattern of nucleation, clearly aligned with the ridges machined in the substrate. Fine surface dendrites nucleated along the ridges, appeared to have grown nearly perpendicular to the ridge. These microstructures also indicate some reduction in nuclei spacing along the ridge with increased sulphur although, relative to smooth substrates, the effect appears to be minor. Four areas from the surface of each sample were randomly selected for nucleation frequency counting and the average nucleation density, expressed as number of nuclei per mm^2, was used in the detailed quantitative analysis.

The transient heat flux, calculated for each immersion experiment using the measured substrate temperatures, rose to a maximum value within the first ten milliseconds or so of contact, the critical period for establishing the melt/substrate contact. Results presented in Figs. 3 (a) and (b), obtained from experiments performed with sulphur contents of 0.006 to 0.05 wt% using both the smooth and the ridge textured substrates, illustrate this behaviour. It proves useful to characterise each experiment by the peak heat flux, as a quanti-

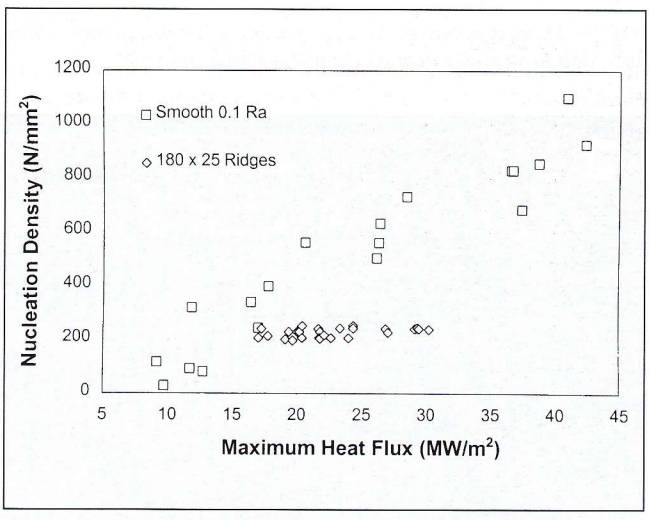

Fig. 4 Maximum heat flux vs. surface nucleation density correlation for samples solidified on smooth and ridge textured substrates under various experimental conditions

Fig. 4 Correlazione fra massimo flusso di calore e densità della superficie di nucleazione per campioni solidificati su substrato liscio e rugoso in diverse condizioni sperimentali

tative reflection of the effectiveness of the initial melt/substrate contact. It can be seen from Fig. 3 that sulphur has a significant impact on the maximum heat fluxes, particularly with the smooth substrate.

Maximum heat flux and nucleation density values measured from the experiments carried out with both smooth and ridge textured substrates are correlated in Fig. 4. These results include all of the data obtained under the range of experimental conditions, covering sulphur levels, Cr/Ni ratios and pool gas atmosphere. By varying contacting effectiveness, primarily through sulphur additions, the maximum heat flux for the smooth substrate was found to increase from around 10 to 40 MW/m^2, with a corresponding linear increase in the nucleation density from around 50 to 1000 nuclei/mm^2. For the textured substrate, the maximum heat flux varied over a smaller range, with changes in process conditions, from around 17 to 30 MW/m^2. In this case the nucleation density remained essentially constant around 200 to 250 nuclei/mm^2. Clearly with textured substrate surfaces, the nucleation pattern is predominantly imposed by the texture itself, rather than by the process conditions.

Microstructure Characterisation of Solidified Sections

Typical solidification structures, shown in Figs. 5 (a) and (b), were obtained from the transverse sections (i.e., cross sections in the plane normal to the casting direction) of the samples solidified on smooth and ridge textured substrates with a melt containing 0.015 wt% sulphur. It can be seen that the solidification structures were fine in the vicinity of the surface in contact with the substrate and became progressively coarser as fully columnar growth was established away from the melt/substrate interface. Typically, the primary dendrite arm spacing increased from around 5 μm near the substrate side to around 30 μm near the melt side and the secondary dendrite arm spacing values were in the range of 3 to 8 μm. The measured secondary arm spacing values are consistent with the measurements reported by other researchers (10,11,12), and are around an order of magnitude finer than the typical secondary arm spacings reported for conventional thin and thick slab casting processes.

Delineating the austenite grain structure is difficult from the microstructures presented in Figs. 5 (a) and (b), perhaps only by inference from the boundaries of aligned dendrites. However, the austenite grain boundaries could be more clearly seen at a higher magnification (at least 500 times) on lightly etched samples. Two such microstructures, presented in Figs. 6 (a) and (b), correspond to Figs. 5 (a) and (b) respectively. These microstructures show only the regions near the substrate side and the grain boundaries have been manually highlighted to enhance the grain delineation. Electron Back Scattered Diffraction measurements confirmed that these were indeed distinct grains of different orientation (13). The austenite grains, in general, were observed to be coarse and columnar.

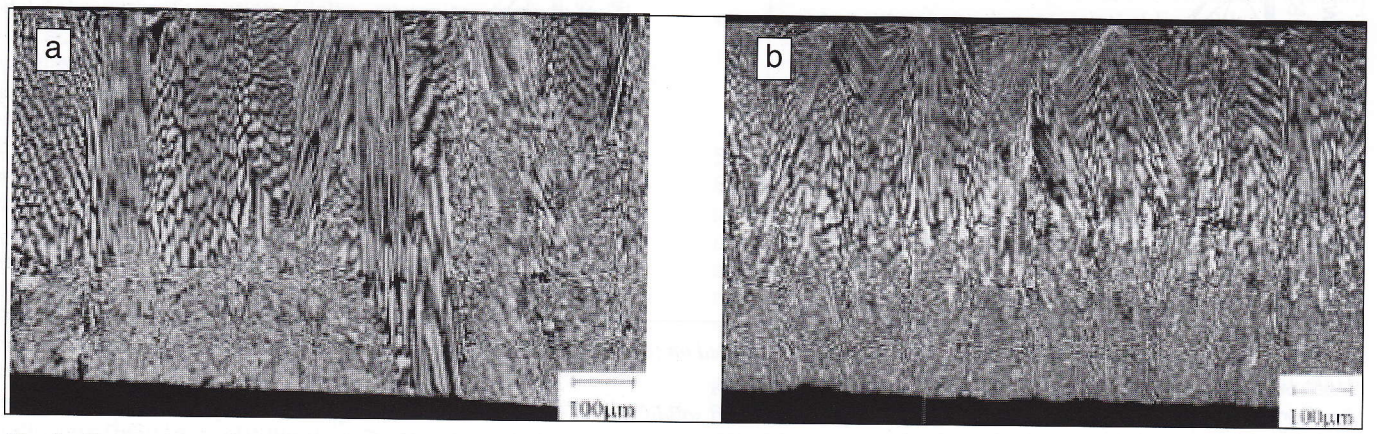

Fig. 5 - Transverse section microstructures of the samples (0.015 wt% S) solidified on (a) smooth and (b) ridge textured substrate surfaces indicating through-thickness dendritic structure

Fig. 5 - Microstructure della sezione trasversale di campioni (0,015 peso % S) solidificati su (a) superficie di substrato liscio e (b) rugoso indicanti la struttura dentdritica attraverso lo spessore

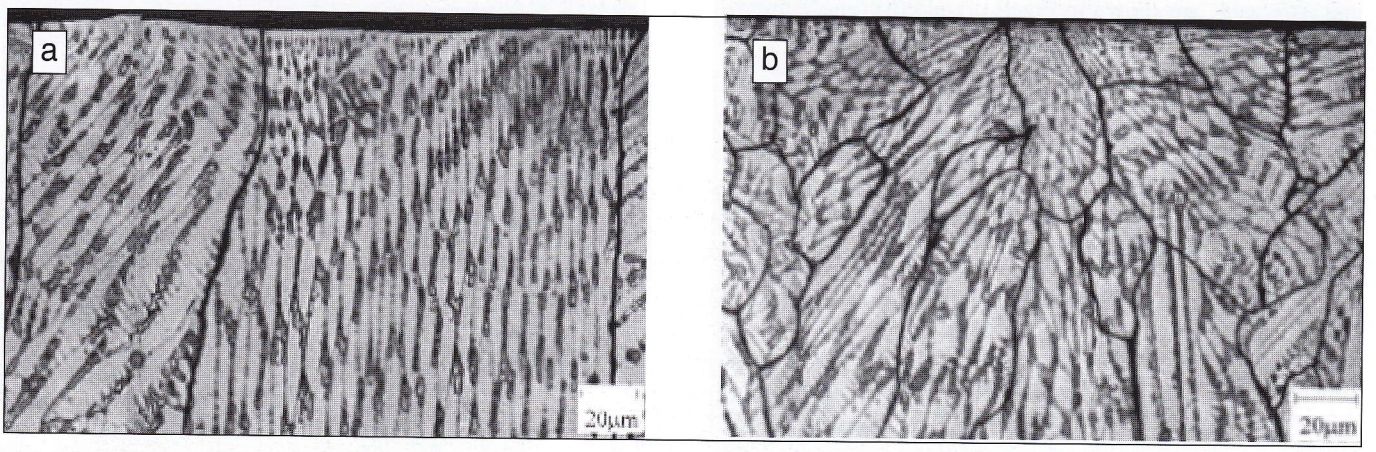

Fig. 6 - Transverse section microstructures of the samples (0.015 wt% S) solidified on (a) smooth and (b) ridge textured substrates indicating the austenite grain structure of the substrate side region (Note that the grain boundaries have been highlighted for clear delineation)

Fig. 6 - Microstructure della sezione trasversale di campioni (0,015 peso % S) solidificati su (a) superficie di substrato liscio e (b) rugoso indicanti la struttura austenitica del grano della regione laterale del substrato (I bordi dei grani sono stati evidenziati per una più chiara delineazione)

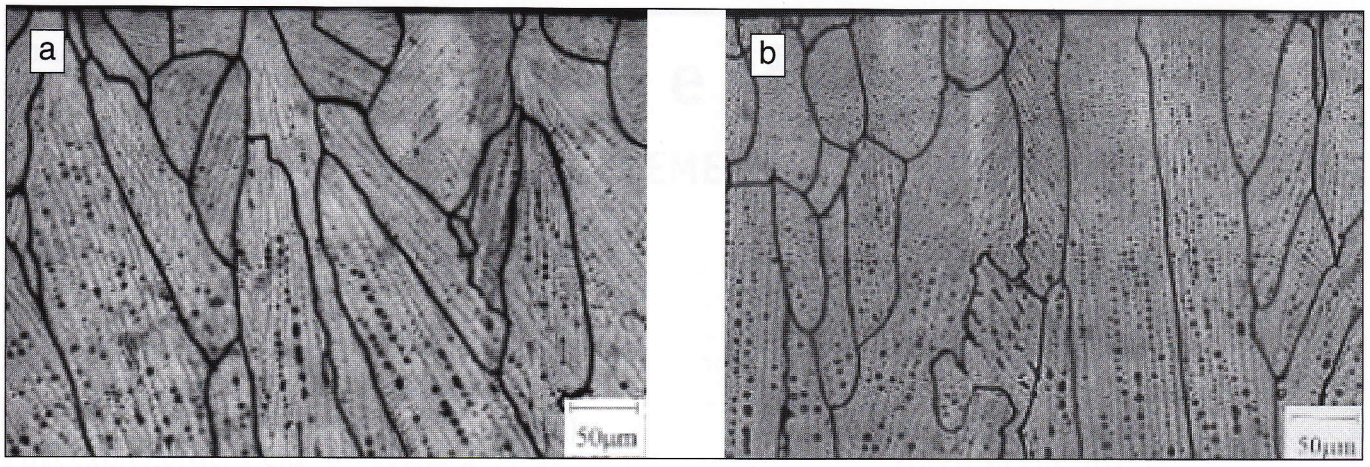

Fig. 11 - Transverse section microstructures of the samples (0.02 wt% S) solidified on (a) 200x28 µm and (b) 75x25 µm pyramid substrate surfaces indicating the austenite grain structure of the substrate side region (Note that the grain boundaries have been highlighted for clear delineation)

Fig. 11 - Microstrutture della sezione trasversale dei campioni (0.02 peso % S) solidificati su una superficie di substrato con textura piramidale di (a) 200x28 µm e (b) 75x25 µm indicanti la struttula del grano austenitico della regione laterale del substrato (I bordi del grano sono stati evidenziati per una migliore delineazione)

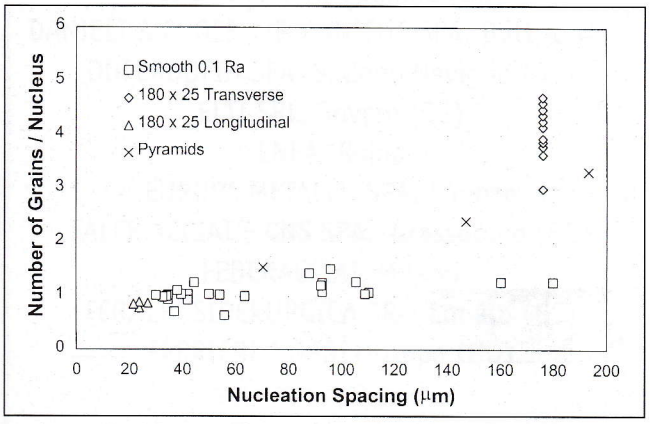

Fig. 12 - Correlations between nucleation spacing and number of grains per nucleus for samples solidified on smooth, ridge textured and pyramid textured substrate surfaces under various experimental conditions

Fig. 12 - Correlazioni fra spaziatura di nucleazione e numero di grani per nucleo per campioni solidificati su superfici di substrato liscio, rugoso e con textura piramidale in diverse condizioni sperimentali

stuctures were similar. The dendritic structure produced from the coarse pyramid substrate exhibited pronounced fanning features and multiple grain formation as was the case with the transverse section of the samples solidified on the 180x25 µm ridge textured substrate. However, for the finer pyramid substrate, there was no significant fanning, and austenite grain widths were found to be similar to the pyramid spacings, as was the case with smooth substrates and for longitudinal sections with ridges.

The results obtained from all of the experiments performed in this study are consolidated in Fig. 12 as a plot of the number of austenite grains per nucleus (contact point) versus the nucleation spacing. For the textured substrates, the grain forming mechanism was found to be a strong function of nucleation spacing. For coarse spacings, as imposed by the ridge substrate with 180 µm pitch or by the pyramid substrate with 200 µm pitch, significant dendrite fanning was observed and this corresponded to the formation of around four austenite grains in the cross-section for each surface nucleation point. As the textures became finer, there was less evidence of dendrite fanning and the number of austenite grains per nucleus progressively decreased, ultimately approaching a 1:1 correlation between grain width and nucleation spacing. For the smooth substrates, dendrite fanning was not observed, and the 1:1 correlation between nucleation spacings and austenite grain widths was essentially maintained over a wide range of contacting conditions. Thermal modelling suggests that dendrite fanning is associated with departures from uni-directional heat transfer near the direct melt-substrate contact points. With smooth substrates the small interfacial gap between the melt and the substrate may explain the relatively uniform heat transfer.

CONCLUDING REMARKS

Experimental studies have demonstrated the importance of melt-substrate contacting conditions, as influenced by substrate textures and melt chemistry, in the evolution of microstructure. A clear link has been identified between nucleation behaviour and austenite grain structures in 304 stainless steel solidifying under conditions that simulate strip casting. This highlights that phenomena taking place in the first few milliseconds of contact between liquid steel and the casting rolls can have a significant bearing on final microstructures and product properties of strip cast materials.

REFERENCES

1) W. Blejde, R. Mahapatra and H. Fukase, Iron & Steelmaker, Vol. 28, (2001), No. 2, p43-48.

2) K. Mukunthan, L. Strezov, R. Mahapatra and W. Blejde, The Brimacombe Memorial Symposium Proceedings, Canadian Institute of Mining, Metallurgy and Petroleum, Vancouver, Canada (2000), p421-437.

3) L. T. Shiang and P. J. Wray, Metall. Trans., Vol. 20A, (July 1989), p1191-1198.

4) A. Mascanzoni, J. M. Damasse, and G. Hohenbichler, Innovation Session, Paper No. 51, CCC 2000, Linz, Austria (June 2000), p1-6.

5) H. Takuda, S. Kikuchi, N. Hatta and J. Kokado, Steel Research, Vol. 62, (1991), No. 8, p346-351.

6) D. Raabe, Materials Science and Technology, Vol. 11, (May 1995), p461-468.

7) L. Strezov and J. Herbertson, ISIJ International, Vol.

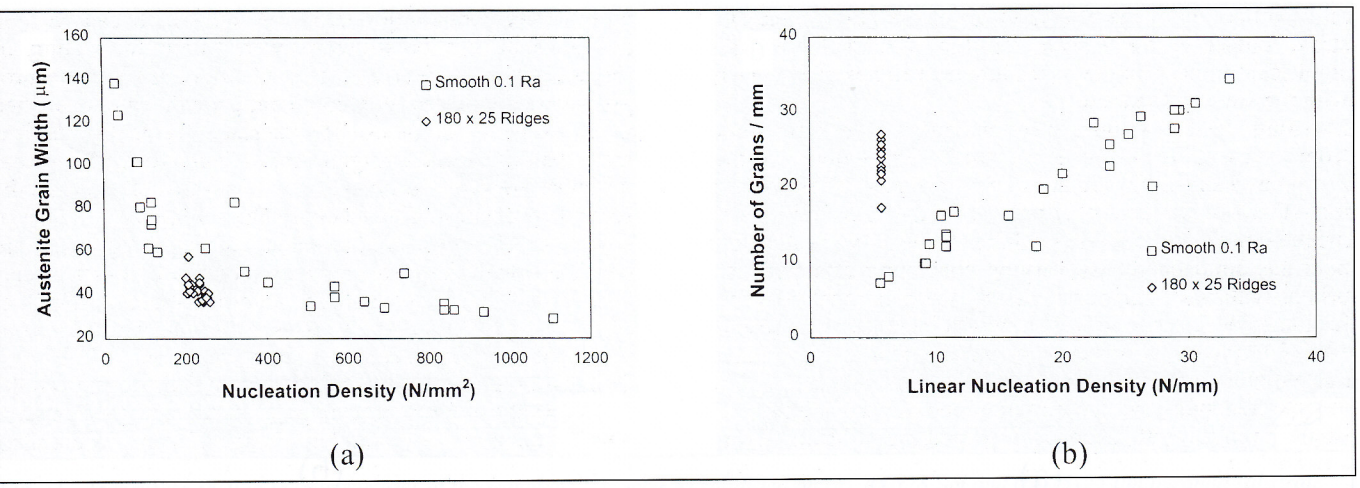

Fig. 7 - (a) Correlations between surface nucleation density and austenite grain width for samples solidified on smooth and ridge textured substrates under various experimental conditions and (b) the same data when correlated as linear nucleation density vs. number of grains per mm

Fig. 7 - (a) Correlazioni fra densità di nucleazione della superficie e larghezza del grano austenitico per campioni solidificati su substrato liscio e rugoso in diverse condizioni sperimentali e (b) gli stessi dati correlati in termini di densità di nucleazione lineare rispetto a numero di grani per mm

The 'length' of the grains in the thickness direction often extended to all or most of the thickness of the solidified sample and did not vary much with processing conditions. It was the 'width' dimension of the grains that changed significantly with solidification conditions. In this study, average austenite grain width values of each sample were measured in a systematic manner by scanning hundreds of grains along a path that is parallel to the chill surface. The grain widths tended to increase somewhat from the substrate side towards the melt side. The values of grain width reported in this paper are taken at a distance of around 50 μm from the chill face.

The nature of the dendritic structure, directionality in particular, and the type of grain development shown in Figs. 5 and 6, are significantly different for the samples solidified on (a) smooth and (b) ridge textured substrates. The dendrites seem to be reasonably perpendicular to the substrate surface for the samples solidified on the smooth substrate, whereas for the samples solidified on the textured substrate, a characteristic fanning type feature could be observed from the points of contact, i.e., from the machined ridge tops. The austenite grain width for the sample solidified on the smooth substrate is quite coarse, consistent with large colonies of dendrites of a single orientation. On the other hand, the fanning dendritic feature observed in the samples solidified on the textured substrate resulted in a multiplication of grains in the vicinity of each contact area, yielding a finer austenite grain structure.

The complete set of measurements of austenite grain widths and nucleation densities is summarised in Fig. 7 (a). These measurements cover all of the experimental conditions including varying substrate surface texture, sulphur levels, Cr/Ni ratios and pool gas atmosphere. The range of austenite grain widths and nucleation densities was quite narrow with solidification on the ridge textured substrate, where the texture dominates nucleation behaviour rather than process conditions. In contrast, process conditions, particularly changes in sulphur content, have a pronounced effect on austenite grain width in samples solidified on the smooth substrate. For example, the microstructure in Fig. 6 (a) corresponds to a sample with relatively low nuclei density, coarse dendrite arm spacings and coarse austenite grain width. This can be rationalised in terms of the higher melt surface tension and reduced melt/substrate wetting with relatively low sulphur content (14). Note that the measured grain width values are consistent with values reported by other researchers (5,15), and are around an order of magnitude finer than the typical grain widths encountered in conventional continuous casting.

The same data, re-plotted in Fig. 7 (b) as linear nucleation density versus the number of grains per mm indicates that, for a smooth substrate, there is essentially a 1:1 correlation between the number of nucleation points and austenite grains. With solidification on the ridge texture surface, there was a fixed nucleation density in the transverse cross-sec-

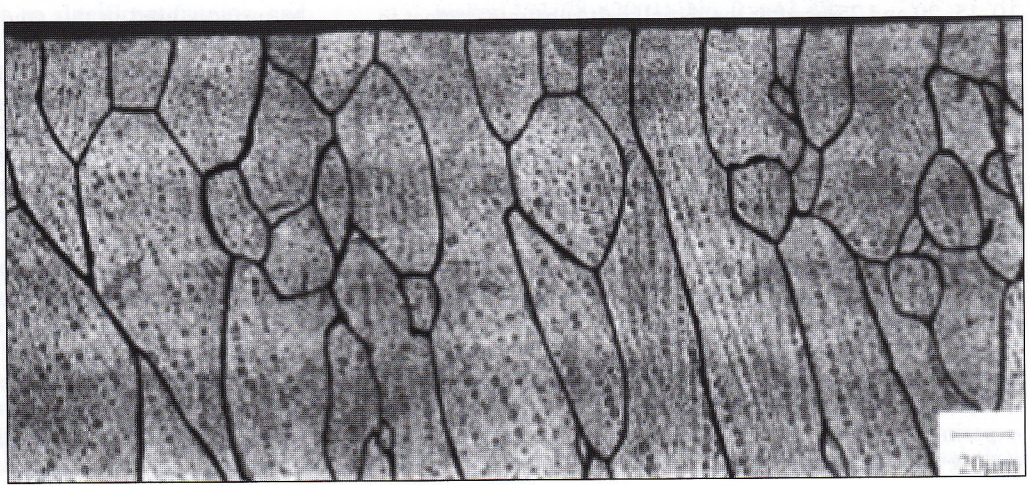

Fig. 8 - Longitudinal section microstructure of the sample (0.015 wt% S) solidified on the ridge textured substrate indicating the dendritic and austenite grain structure of the substrate side region (Note that the grain boundaries have been highlighted for clear delineation)

Fig. 8 - Sezione longitudinale della microstruttura del campione (0,015 peso % S) solidificato sul substrato rugoso indicante la struttura granulare dell'austenite e dendritica della regione laterale del substrato (i bordi dei grani sono stati evidenziati per una migliore lettura.

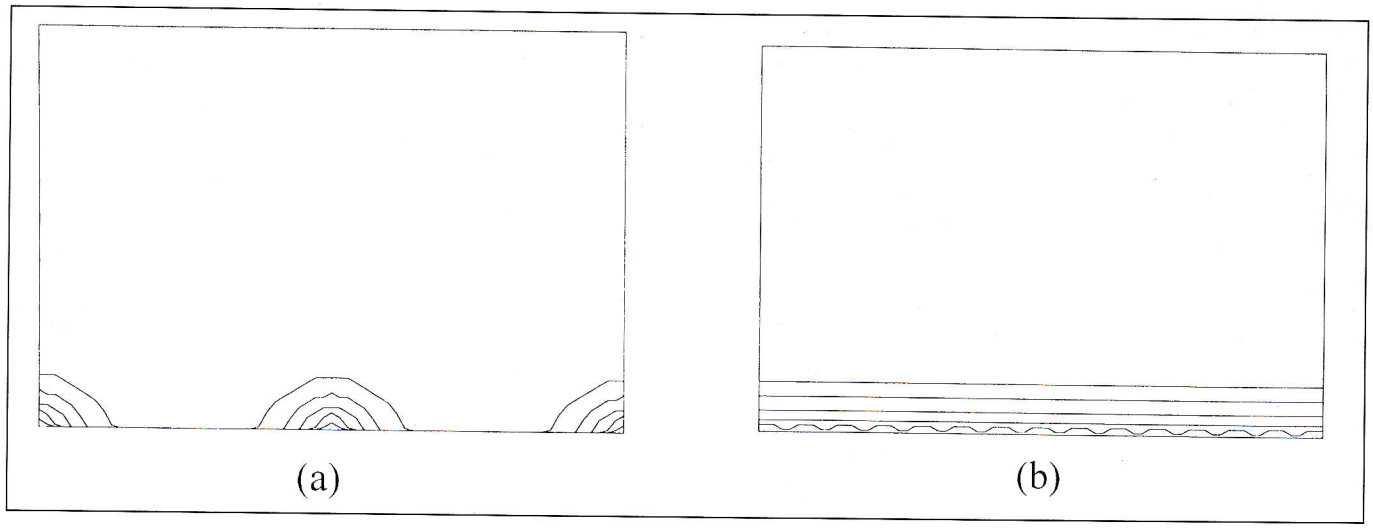

Fig. 9 - Model prediction of the evolution of solid in the (a) transverse and (b) longitudinal cross-sections with the ridge textured substrate at 5, 10, 15, 20 and 25ms after the initial melt/substrate contact

Fig. 9 - Modello previsionale dell'evoluzione del solido nelle sezioni (a) trasversale e (b) longitudinale con il substrato rugoso a 5, 10, 15, 20 e 25ms dopo il contatto iniziale fusione/substrato

tion of about 6 nuclei per mm, which corresponds exactly to the transverse ridge spacing of 180 microns. Moreover, there is a multiplication of austenite grains, in this case 3-4 times more austenite grains than nucleation points. Clearly there is a different mechanism of grain formation for solidification on the smooth and ridge textured substrate, when observed in the transverse section.

The situation was found to be different in the longitudinal direction along the ridges. The microstructure shown in Fig. 8 was obtained from the longitudinal section (i.e., parallel to the substrate ridges and the casting direction) of the sample solidified on the 180x25 μm ridge textured substrate with a melt containing 0.015 wt% sulphur. Thus the microstructures shown Fig. 8 and Fig. 6 (b) were obtained from the same sample except that they correspond to longitudinal and transverse sections respectively. The key difference between these two microstructures is that the one from the longitudinal section did not exhibit significant dendrite fanning features. The dendrites, as well as the grain boundaries, appear to align almost normal to the substrate surface as was the case with the samples solidified on the smooth substrate (see Figs. 5 (a) and 6 (a)). Moreover, the nucleation spacings and the austenite grain widths are very comparable to each other in the longitudinal section, as was found with smooth substrates, although finer in this case with values of 25 to 30 μm.

In order to explore this further, three-dimensional modelling of heat transfer and early solidification with a 180 μm pitch and 25 μm depth ridge texture was undertaken. The model prediction of the evolution of the solid (solidus lines) at 5, 10, 15, 20 and 25ms after the initial melt/substrate contact in the transverse and longitudinal direction is presented in Fig. 9. The calculated solid evolution patterns are quite consistent with the observation of dendrite fanning in the transverse section, and not in the longitudinal direction along the ridges. In the transverse cross-section there is more persistent departure from uni-directional heat transfer around the contact points.

Microstructure Observations with Specially Designed Substrate Surfaces

Microstructure observations suggest a link between dendrite fanning and multiple grain formation in the transverse sections of samples solidified on the ridge textured substrate. In order to clarify the effect of contact spacing, a special set of experiments were designed, which would impose fixed contacting conditions and spacings in both the transverse and

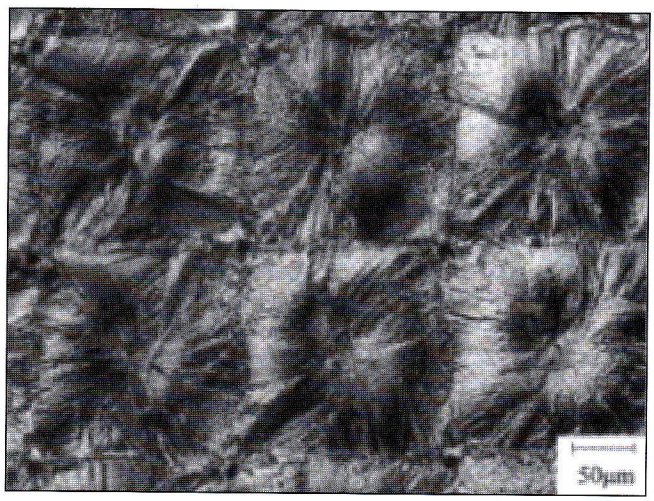

Fig. 10 - Surface solidification structure of the sample solidified on the 200x28 mm pyramid surface texture (0.02 wt% S)

Fig. 10 - Struttura della solidificazione della superficie di un campione solidificato su una superficie con textura piramidale di 200x28 mm (0,02 peso % S)

longitudinal directions. The pyramid surface texture designed for this purpose, details of which have previously been presented (16), had well defined pitch and depth in both dimensions together with small flat top areas that would be available to be fully contacted by the melt. Pyramid substrate surfaces used in this study were of the type 200x28 μm, 150x20 μm and 75x25 μm; the dimensions 200, 150 and 75 μm correspond to pitch and the dimensions 28, 20 and 25 μm correspond to depth. Surface solidification structures of the samples solidified on the pyramid substrates indicated that each pyramid top resulted in a single nucleation point. The imprint of the pyramid dimensions could be seen on the surface structures of the samples as can be seen in Fig. 10, which was obtained for the 200x28 μm pyramid substrate with the melt containing 0.02 wt% sulphur. Samples produced from other pyramid substrates had similar features except that the nucleation spacing was determined by the pyramid dimensions.

Microstructures of the cross-sections of the solidified samples were analysed and the examples presented in Figs. 11 (a) and (b) correspond to the pyramid substrates of 200x28 μm and 75x25 μm respectively. Transverse and longitudinal

38, (1998), No. 9, p959-966.

8) G. K. Allan, Ironmaking and steelmaking, Vol. 22, (1995), No. 6, p465-477.

9) J. A. Brooks and A. W. Thompson, International Materials Reviews, Vol. 36, (1991), No. 1, p16-44.

10) M. Tsukigahora, K. Yamada, M. Mohri, H. Sakaguchi, K. Sasaki, K. Fukuda and N. Nishimae, Intern. Conf. on New Smelting Reduction and Near Net Shape Casting Technologies for Steel, Korean Inst. of Metals, Pohang, Korea (1990), p550-559.

11) T. Mizoguchi and K. Miyazawa, ISIJ International, Vol. 35, (1995), No. 6, p771-777.

12) A. Kasama, S. Mizoguchi, K. Miyazawa, M. Ito and T. Sugai, Trans. ISIJ, Vol. 26, (1986), pB139-B140.

13) A. Hunter, Ph.D. Thesis (In Preparation), University of Wollongong, Wollongong, Australia.

14) T. Evans and L. Strezov, Metall. and Mat. Trans. B, Vol. 31B, (Oct. 2000), p1081-1089.

15) T. Suzuki, J. Harase, K. Ohta and T. Takesita, Trans. ISIJ, Vol. 28, (1988), pB104.

16) L. Strezov, J. Herbertson and G. R. Belton, Metall. and Mat. Trans. B, Vol. 31B, (Oct. 2000), p1023-1030.

ABSTRACT

EVOLUZIONE DELLE MICROSTRUTTURE DURANTE LA SOLIDIFICAZIONE DI ACCIAIO INOSSIDABILE AUSTENITICO 304

Ai fini della commercializzazione dei nuovi processi di colata di nastri è importante comprendere l'evoluzione delle microstrutture durante la solidificazione.
Questo studio ha esaminato la solidificazione in condizioni di laboratorio controllate elaborate per simulare la regione di menisco e metallo liquido di una macchina di colata a due rolli accoppiati.
E stato riscontrato un legame consistente fra trasferimento di calore iniziale, nucleazione superficiale e conseguente microstrutture che suggerisce che il controllo delle condizioni del contatto iniziale metallo fuso/substrato e del trasferimento di calore sono di primaria importanza nel controllo delle microstrutture finali. Ciò è stato dimostrato a livello sperimentale durante la solidificazione di acciaio inossidabile 304 mediante gli effetti di diverse texture di superficie del substrato e l'influenza di solfuro attivo di superficie sulle microstrutture. I grani di austenite hanno mostrato forme colonnari allungate costituite da famiglie di dendriti formate sul lato opposto della direzione locale del flusso di calore. La larghezza dei grani di austenite rifletteva quasi la spaziatura di nucleazione delle superfici, tipicamente con un rapporto 1:1 e in alcuni casi una moltiplicazione dei grani associata a campi termici non uniformi intorno ai punti di contatto.